How Chemical Environment Activates Anthralin and Molecular Oxygen for Direct Reaction

Emerald S. Ellis, Luke T. MacHale, Robert K. Szilagyi,* Jennifer L. DuBois*

Department of Chemistry and Biochemistry, Montana State University, P.O. Box 173400, Bozeman, MT 59717 U.S.A.

ABSTRACT:

The role of the chemical environment in promoting anthralin/O_2 reactions was discovered, using neat solvents to model the amino acids of a cofactor-independent oxygenase. Experimental and computational results highlight the importance of the substrate-enolate, which is accessed via energetically small, escalating steps in which the ground state keto-isomer is tautomerized to an enol and then ionized by solvent. The resulting ion-pair is poised for spontaneous electron transfer to O_2. Similar activation may be exploited in biological/non-biological oxidations involving O_2.

Enzyme active sites use particular arrangements of amino acids to catalyze many reactions with efficiencies and specificities not yet achieved by synthetic catalysts. Reactions between organic molecules and dioxygen (O_2) are often thermodynamically favorable, but the triplet ground state of O_2 imposes a significant kinetic barrier.[1] Nearly all enzymes that use this desirable "green" oxidant[2] need metabolically expensive flavin or redox-active transition metal cofactors to reductively activate O_2.[1,3] Cofactor-Independent Oxidases (CIOs) catalyze oxidations of organic substrates by O_2 using only intermolecular interactions supplied by the protein environment (Figure 1).[4] The exact mechanisms of substrate binding and catalysis are unknown, but previous work suggests protein/substrate interactions play a key role by tuning the substrate's O_2-activating efficiency.[4-7] The oxygenation of dithranol (also known as anthralin or 1,8-dihydroxy-9,10-dihydroanthracen-9-one, CAS# 1143-38-0) to dithranone (Scheme 1A) is catalyzed by a CIO involved in anthracycline biosynthesis called nogalamycin monoxygenase (NMO, Figure 1).[8-10] This reaction also occurs in an uncatalyzed manner when dithranol is used topically to treat psoriasis. The mechanism of action is not well understood but is surmised to be related to the generation of reactive oxygen species by dithranol, analogous to the initial step shown in Scheme 1A.[11]

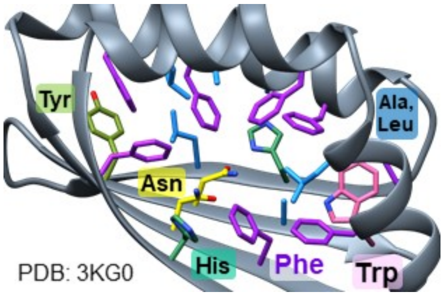

Figure 1. Crystal structure of cofactor-free nogalomycin monooxygenase, showing amino acid side chains lining the active site pocket. Table S1 shows proposed solvent/amino acid side chain correlations and solvent physical properties.

Our approach is to use neat solvents to deconvolute the network of supramolecular interactions between substrate, O_2, and the substrate binding pocket of a CIO (Table S1) by probing how solute/solvent interactions influence the reactivity of dithranol. It is relevant to structure/function considerations that molecules of this class can assume a remarkably large variety of tautomeric structures and be strongly influenced by modest variations in chemical environment. Three complementary spectroscopic techniques and a validated level of computational theory (Tables S2-S4) were employed to explore how each solvent environment, acting as a model for a type of substrate/amino acid interaction,[12,13] influences dithranol structure and relative isomer energies to activate the dithranol/O_2 pair toward spontaneous electron transfer.

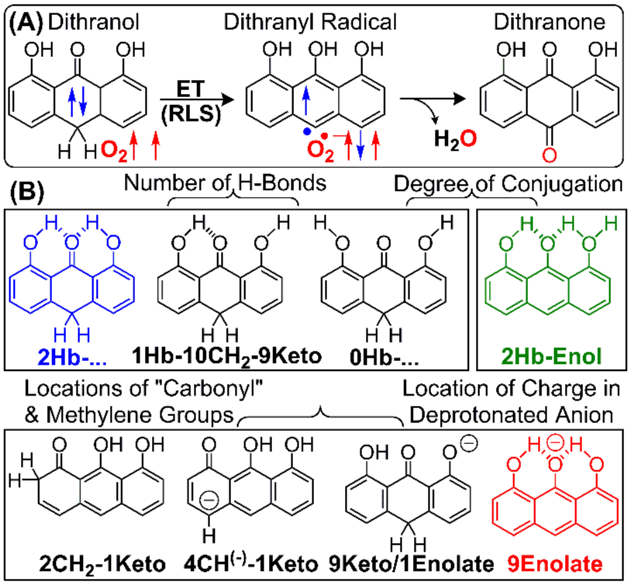

Scheme 1. (A) NMO-catalyzed oxygenation of dithranol with (B) a representative set of potentially accessible tautomers. Lowest-energy isomers of the three main forms of dithranol are colored: blue = keto; green = enol; red = anion (enolate). For full set of isomers see Scheme S1.

Our results indicate that ion-pairing between an enolate isomer and protonated solvent molecules is critical for stabilizing the reactive substrate anion along the way to form an enolyl/superoxide radical pair (Scheme 1A). This result is unexpected because the structure of the reactive dithranolate anion is often predicted to be a C10 carbanion due to the weak C-H bond.[14] Additionally, prior theoretical investigations[13,14] strongly favor dominance of the keto isomer in neat solvents, contrary to our experimental observations. The mechanism invoked here was initially inspired by how flavin-dependent oxidases prime the reduced flavin to activate O_2.[3] In subsequent experimental work under semi-aqueous conditions (2:1 Tris/NaCl buffer:2-methoxyethanol [2ME], pH 8), only the anionic form of dithranol reacted appreciably with O_2,[6] suggesting that the enolate is activated to form the experimentally detectable dithranyl/superoxide ($O_2^{\bullet -}$) radical pair in a rate-determining step. Following intersystem crossing, the radical pair generates the oxygenation product (dithranone) and water (Scheme 1A).[6,7]

The presence of enolate likewise correlated with rapid reaction between dithranol/O_2 in neat solvents. For example, dithranol in $CHCl_3$ (100% ketone, Figure 2) did not react with O_2 within 48h. By contrast, the half-life for the same reaction in DMF (100% enolate, Figure 2) was 2.9h (Figure S1). Oxygen is more soluble in $CHCl_3$ than DMF (Table S1), suggesting that the discrepancy can be ascribed to the intrinsic reactivity of the dithranol/O_2 pair,[15] which in turn correlates with the presence of the enolate. The pK_a of 9.28±0.07 measured for the dithranol ⇄ enolate + H^+ equilibrium in water decreased by two units (7.15±0.09) for NMO-bound dithranol, indicating that the protein stabilizes the enolate (Figure S2). To understand how, we first considered the structure of the substrate dithranol (Scheme S1) in light of its array of C-H/O-H bond tautomers, methylene positional isomers, ionization isomers, and varied intramolecular H-bonding patterns. While in the gas phase these were calculated to span a *ca.* 200 kJ·mol^{-1} relative energy range (Figure S3) using validated density functional theory, the energetic order may be readily altered by the protein environment toward promoting deprotonation and reaction with O_2. The level of theory (MN15[16]/6-311++G**[17-19]/SMD[20,21]) was validated using CBS-Q3 results[14] from the literature (Table S2).

To understand the activating effects of the chemical environment, we used UV/visible absorbance (UV/vis), fluorescence, and proton nuclear magnetic resonance (^{1}H-NMR) spectroscopies to determine the most stable isomer(s) of dithranol in a series of solvents chosen based on the side chains in NMO (Figure 1, Table S1). The results indicated a spontaneous shift from the pure dithranol-keto isomer in $CHCl_3$, benzene, and H_2O, to keto:enolate mixtures in 2ME and DMSO (80:20 and 70:30), to apparently pure enolate in DMF (Figures 2, S4-S7, Tables S5-S6). NMR characterizations were limited by the tendency of isomer mixtures to change in composition between solute concentrations typical of NMR (≥1 mM) and concentrations used to investigate the enzyme (≤300 μM). We speculate that solute-solvent intramolecular interactions predominate over solute-solute interactions only at lower solute concentrations. Additionally, the use of infrared spectroscopy was prohibited by the overlap of diagnostic carbonyl and C=C stretches for these tricyclic aromatic molecules. These challenges may have precluded observation of the enolate in prior experimental studies, in which it has long been assumed that keto isomers of anthralin exclusively constituted the ground state.

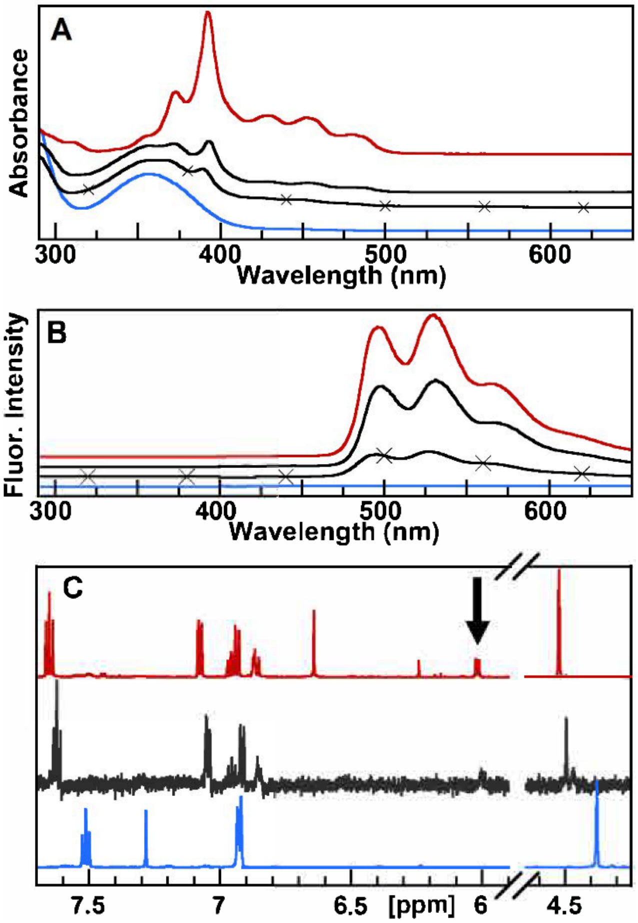

Figure 2. Representative spectra demonstrating solvent-dependent stabilization of dithranol isomers. (A) UV/vis spectra of 50 µM dithranol in $CHCl_3$ (blue, keto form), DMF (red, enolate), DMSO (black solid lines, 70:30 keto:enolate mixture), and 2ME (black (x), 80:20 keto:enolate mixture (Figure S5). **(B)** Fluorescence spectra of 50 µM dithranol in $CHCl_3$ (blue, $\lambda_{exc.}$=380 nm), 5 µM dithranol in DMSO (black, $\lambda_{exc.}$= 393 nm), 5 µM dithranol in 2ME (black (x), $\lambda_{exc.}$= 393 nm) and DMF (red, $\lambda_{exc.}$= 391 nm). The fully conjugated, aromatic enolate isomer fluoresces strongly, while the keto does not (Figure S6). **(C)** ^{1}H-NMR spectra of dithranol in $CDCl_3$ (blue, 10 mM), d^6-DMSO (black, 0.16 mM), and d^7-DMF (red, 0.32 mM). The black arrow indicates a doublet in the region expected for aromatic protons, absent in the blue spectrum and tentatively assigned to the proton on the fully conjugated central ring of the enolate isomer. (See also Figure S7.) Dithranol yields equivalent keto spectra in all three solvents at concentrations >1 mM (not shown).

The tendency to shift from predominantly keto to the reactive/charged enolate does not correlate straightforwardly with solvent (**S**) polarizability as expressed by the dielectric constant (Table S1). Water, for example, with the highest dielectric constant, overwhelmingly favors the keto form. Instead, enolate stabilization correlates with a combination of parameters including H-bond acceptance (β), zwitterionic character, and π/π-stacking, in addition to the dielectric constant (Table S1). The solvents with the greatest enolate content (DMF > DMSO = 2ME) share high β-values (0.7-0.9, Table S1). Each can adopt a zwitterionic resonance form stabilized by accepting a proton at an oxygen (DMSO, 2ME) or nitrogen (DMF) lone pair, forming a protonated solvent cation (**S**H^+). The zwitterionic form of these solvents draws a parallel to the imidazole side chain of histidine, which accepts a proton to form cationic imidazolium[5] that can in turn interact with a substrate anion.[22] Solvents with a π-electron cloud (benzene, DMF, DMSO) could form energetically significant π/π-stacking interactions that are further elaborated by the stacking of dithranol molecules in its crystal structure.[23]

In parallel to experiments, we calculated Gibbs free energy diagrams for the lowest energy dithranol isomers and their ionized forms as solutes in order to establish an atomic-scale description of how solvents may activate dithranol solute. Figure 3 and Table S3 present the condensed-phase translational entropy-corrected[24] (Table S4) Gibbs free energy (ΔG^{corr}) diagram for models including both explicit solvent molecules and polarizable continuum environments.[20,21] For clarity, we only show the lowest energy/predominant keto and enol tautomers, a transient state with an inverted H-bonding pattern of deprotonated dithranol and protonated solvent (when structurally available), and the ionized form (Figure S3, red lines). In the latter, we evaluated supramolecular assemblies where the protonated solvent rests near the anionic solute molecule, forming stable (enolate$^-$):(**S**H^+) ion-pairs.

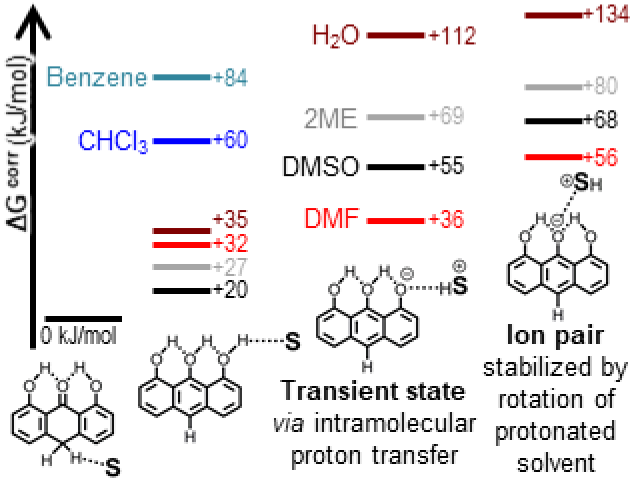

Figure 3. The condensed-phase translational entropy corrected Gibbs free energy (ΔG^{corr}) diagram is shown for the lowest energy keto, enol, and transient and stationary enolate isomers of dithranol. Explicit solvent and protonated solvent molecules are embedded in a polarizable solvent environment. Transient state geometry was fixed by keeping the distances between the ionized dithranolate-O^- and protonated solvent fixed with an imaginary normal mode along the (C-O^-)···H**S**$^+$ interaction path.

It is important to highlight that, independent of the level of theory or the solvation model, the crystallographically characterized keto form[23] was the most stable isomer. Depending on their H-bond acceptor and π/π-stacking properties, explicit solvent molecules either stack with dithranol or form significant (10-20 kJ/mol) C-H···Cl/N/O interactions with the solute. All considered keto models (Figure S8) were constructed with the energetically most favorable methylene group/solvent interactions. The most stable form of the neutral enol (still higher in energy than the keto forms) had two intramolecular H-bonds between a peripheral and the central phenol groups, while the third, dangling peripheral O-H bond provided a H-bond donor to solvent (Figures S8-S9).

Solvents with nucleophilic O/N (DMSO, DMF, H_2O, 2ME) showed less than 35 kJ·mol^{-1} endothermicity in forming the solvent/enol isomer supramolecular assembly. The lower energy block of (enol-O-H)×(**S**) tautomers (Figure S3) was followed by the chloroform adduct due to a dithranol-O(H)···H-CCl_3 interaction. Benzene formed an O-H···π-cloud interaction at the peripheral phenol group (Figure S10). The modest energy gap between the keto×(**S**) and enol×(**S**) tautomers thus defines a thermodynamically accessible stepping-stone toward ionization of the dithranol substrate, leading to the key dithranyl•/O_2•⁻ radical-pair intermediate (Scheme 1A).

A transiently ionized dithranol state was generated by inverting the H-bonding pattern (enol-$O^{\delta-}$-H···$\mathbf{S}^{\delta+}$) between the solvent molecule's nucleophilic center and the peripheral phenol group (Figures S10-S11). This is another critical stepping-stone toward the enolate-O^-···H-$\mathbf{S}^+$ ion-pair, where the relative Gibbs free energies for each state correlate with the thermodynamic stability of the protonated solvent molecule. The two lowest energy structures were calculated for the $DMFH^+$ and $DMSOH^+$ (Figure S12) supra-molecular assemblies with the enolate. These solvents also form the most stable zwitterions, through which they are primed to accept H^+.

SH^+ was rotated above the dithranol/enolate plane to prevent spontaneous back-transfer of the proton from **S**H^+ to the phenolate group. The fully ionized, deprotonated enolates with equilibrium structures (Figure S12) adopt a highly similar H-bonding pattern to the neutral keto form (Figures S11-S12). The ion-pair is stabilized by a short-range Coulomb interaction. The relative Gibbs free energy values shift upward in energy by only *ca.* 20 kJ·mol^{-1} (Figure 3). Most of the ion-pairs remain within the energy range that can be considered reasonable (~100 kJ·mol^{-1}) for observing spontaneous reactivity under ambient conditions.

The experimentally observed reactivity patterns (Figure S1)[6] can be explained in part using the computational models. Lack of reactivity in chloroform and benzene suggests that neither the keto tautomer nor the explicitly solvated enol, which is energetically accessible from the keto, is likely to be sufficiently activated for dioxygen reactivity.[1] Aqueous/2ME[6,7] and DMF are optimal due to reasonable O_2 solubility (Table S1) and strong stabilization of the enolate and **S**H^+. Despite the favorable energetics for the enolate/**S**H^+ ion-pair, low O_2 solubility hinders reactivity in DMSO. The low O_2 solubility and energetically unfavorable zwitterionic form of water further poses a challenge for achieving aqueous reactivity.

An activated enolate/**S**H^+ ion-pair is generated through a series of endothermic yet energetically attainable steps under ambient conditions, beginning with the conversion of the keto to an enol tautomer. Conversion of the enol to the ion-pair via an appropriate solvent/sidechain yields an energized intermediate, which may serve the role of a transition state from which activation of O_2 to $O_2^{\bullet-}$ by the substrate anion may occur. We envision similar steps in the NMO active site that may increase the rate of substrate oxidation over 2,000-fold relative to the non-catalytic process.[6] These results also suggest a mechanism whereby anthralin derivatives, delivered topically in organic matrices as psoriasis drugs or systemically as chemotherapeutics, may react with O_2. The principle of cooperation between substrate/solvent to form an ion-pair that converts to the reactive radical pair could be exploited in some organic transformations in which O_2 is the desired oxidant.[25]

EXPERIMENTAL

Solvents and Reagents. All reagents and solvents were purchased commercially and used without further purification. Acidic DMSO ($DMSO_{Acid)}$ was prepared by adding concentrated HCl (12.18 M, 37 w/w%) to DMSO to a final concentration of 1 mM. Alkaline DMSO ($DMSO_{Alk}$) was prepared by adding NaOH from a concentrated solution (12.18 M, 39 w/w%) in deionized water to DMSO to a final concentration of 1 mM. Acidic and alkaline 2ME ($2ME_{Acid}$ and $2ME_{Alk}$) were prepared similarly. Aqueous buffers containing 100 mM buffer and 300 mM NaCl were adjusted to the following pHs with 5 M HCl or NaOH: citric acid/trisodium citrate (pH 5.02, 5.53, 5.97), *N,N-bis*(2-hydroxyethyl)-2-aminoethanesulfonic acid (BES) (pH 6.50, 7.00, 7.54), tris(hydroxymethyl)-aminomethane (tris/tris-HCl) (pH 8.06, 8.43), *N*-cyclohexyl-2-aminoethanesulfonic acid (CHES) (pH 8.90, 9.54), and *N*-cyclohexyl-3-aminopropanesulfonic acid (CAPS) (pH 9.95, 10.47, 11.15). Solvents and aqueous buffer solutions used for anaerobic experiments were degassed by repeatedly freezing and thawing under vacuum with argon purge, except for DMSO and 2ME, which were degassed by repeated vacuum/Ar purge cycles, and DMF, deuterated $CHCl_3$, and deuterated DMSO, which were oxygen-free as purchased and stored in a dry anaerobic chamber (MBraun). Dithranol stock solutions were prepared in degassed, HPLC-grade DMSO and transferred via gas-tight syringe to crimp sealed amber vials. Stock concentrations were measured by UV/vis in $DMSO_{Acid}$: $\varepsilon_{356nm} = 7.83 \pm 0.03$ $mM^{-1}cm^{-1}$. Stocks of the product dithranone (1,8-dihydroxy-9,10-anthracenone) were prepared in DMSO.[26]

Expression and Purification of NMO. The gene encoding the N-terminally His_6-tagged NMO (pBad vector) was received as a kind gift from the Schneider laboratory, University of Turku, Finland.[10] The NMO was expressed and purified as described previously.[6] For anaerobic experiments, NMO was purged of O_2 by gently stirring on ice in an anaerobic chamber for 30-40 min.

UV/Visible (UV/vis) Absorbance Spectroscopy. UV/Vis spectra were measured using a Varian Cary50 spectrophotometer under ambient conditions and plotted/analyzed using Kaleidagraph 4.0 (Synergy Software, Reading, PA). Samples of dithranol were prepared by adding dithranol from a concentrated stock to solvent in an unsealed cuvette because, with the exception of aqueous buffers and alkaline solvents, no oxidation products were detected on the timescale of the measurements. Samples of dithranol in alkaline solvents and aqueous buffers were prepared by sealing degassed solvent into a cuvette in an anaerobic chamber (Coy) and adding dithranol to the sealed cuvette via gas tight syringe. Quartz or glass cuvettes were used for all measurements for broader solvent compatibility.

Fluorescence Spectroscopy. Fluorescence emission spectra were measured in quartz cuvettes using an Agilent Cary Eclipse spectrophotometer. Solutions of dithranol in various solvents were prepared as described for UV/vis spectra measurements. Excitation wavelengths were chosen based on the wavelengths of maximum absorbance in the fluorescence excitation spectrum when emission at 495 nm is monitored ($CHCl_3$ and benzene, 380 nm; H_2O, 383 nm; 2ME, 389 nm; DMF, 391 nm; DMSO, 393 nm).

Nuclear Magnetic Resonance (NMR) Spectroscopy. NMR spectra were obtained using a Bruker 600 MHz Avance III spectrometer. Solutions of dithranol or dithranone were prepared gravimetrically by dissolving the solid into deuterated solvent ($CDCl_3$, $(CD_3)_2SO$, or $(CD_3)_2NCDO$) in a dry anaerobic chamber (MBraun) and sealing the tube with a plastic cap. Low-concentration samples were prepared by serial dilution with deuterated solvent in a dry anaerobic chamber.

Aqueous Spectrophotometric pH Titrations. The UV/Vis spectra of free dithranol and the dithranol:NMO complex as a function of pH were measured as described above. All pH titrations were performed by a discontinuous method using a different aqueous buffer for each pH (see above) due to instability of the enzyme when concentrated acid or base is added. To determine a pK_a for dithranol in the absence of enzyme a 46 μM dithranol solution in aqueous buffer was prepared anaerobically at each pH >7.5, and its absorbance spectrum measured. Because of dithranol's poor solubility in neutral and acidic aqueous solution, the pKa for the dithranol:NMO complex was determined by first adding a stoichiometric excess of NMO (80 μM) anaerobically to each solution, before adding 39 μM dithranol. The solutions were incubated for 5 min before the absorbance was measured.μ

Values for pK_a were determined by plotting the absorbance at 385 nm (λ_{max} for dithranolate anion) or 393 nm (λ_{max} for dithranolate:NMO complex) as a function of pH and fitting the data to a curve (Kaleidagraph 4.0) describing a single pK_a transition:

$$y = (B \times 10^{-pH} + A \times 10^{-pKa})/(10^{-pH} + 10^{-pKa}) \qquad (1)$$

where *A* and *B* are the highest and lowest absorbance values, respectively, extrapolated by the fit.

Estimation of Autoionization in DMSO and 2ME. In both DMSO and 2ME, addition of sufficient concentrated HCl or NaOH fully converts the absorbance spectrum of dithranol to that observed in low- or high-pH aqueous buffer, respectively. UV/Vis absorptivity constants for the fully protonated and deprotonated forms of dithranol (ε_{DH2} and $\varepsilon_{DH(-)}$) were obtained by measuring the absorbance spectra of each at varying concentrations in DMSO or 2ME in the presence of a large excess (1 mM) of concentrated HCl or NaOH. The data were used to generate standard curves ($Abs_\lambda = \varepsilon_\lambda$[Dithranol]) at 1 nm increments over λ = 300-500 nm. These were in turn used to simulate the UV/vis spectrum measured in neat solvent as a linear combination of ε_{DH2} and $\varepsilon_{DH(-)}$:

$$\text{Abs} = (A\cdot\varepsilon_{DH2} + B\cdot\varepsilon_{DH(-)}) \cdot [\text{Dithranol}] \qquad (2)$$

where *A* and *B* represent the mole fraction of protonated and deprotonated dithranol, respectively, and *A + B = 1 (assuming no other speciation is present)*. The fit parameters *A* and *B* were calculated by minimizing the sum-square of the residuals ($\Sigma(Abs_{calc} - Abs_{meas})^2$) over the range of 300-500 nm at 1 nm intervals, using Excel's Solver tool to vary *A + B = 1* (GRG non-linear, default parameters with non-negative *A*, *B*).

Reagent Quantification by High-Performance Liquid Chromatography (HPLC). Quantification of dithranol and its oxygenation product dithranone was performed using an Agilent 1100 LC system (Agilent Technologies, Santa Clara, CA) equipped with a G1315B diode array detector. Each sample or standard was injected at a volume of 20 µL onto a Symmetry C_{18} 5 µm, 4.6 × 150 mm column (Waters) maintained at 50 °C. Solvents used to separate the analytes of interest were (A) water +0.1% (v/v) TFA and (B) acetonitrile +0.1% (v/v) TFA. The separation was carried out with a gradient: 0-3 min (60→90 %B, 1.5→2.5 mL/min), 3-4 min (90→60 %B, 2.5→1.5 mL/min), 4-4.1 min (60 %B, 1.5 mL/min). Analytes were monitored at 354 nm (dithranol) and 430 nm (dithranone). Other oxidation products are not reliably quantified by HPLC. Integrated intensities of the dithranol and dithranone peaks were compared against standard curves to determine concentration.

Uncatalyzed Oxidation of Dithranol in Air. Consumption of dithranol and formation of oxidation products were monitored by UV/vis and discontinuous HPLC as described above. In an anaerobic chamber, 10 mL solutions of 100 µM dithranol in each solvent were prepared in 50 mL round bottom flasks covered with foil to exclude light. Zero-time samples were measured for HPLC and UV/vis analysis before the reaction mixtures were removed from the chamber. The reaction flasks were continuously shaken at room temperature at 100 rpm to establish and maintain air-saturation. Minimal evaporation was observed in most solvents, but reactions in highly volatile solvents such as chloroform were sealed with an ungreased ground-glass stopper between measurements to reduce evaporation. Samples (50 µL) were removed for HPLC and UV/vis analysis at regular time intervals and discarded.

Computational Methods. The X-ray crystal structure of dithranol[23] (REFCODE: ANTHLN) was obtained from the Cambridge Crystallographic Database.[27] The crystal packing informed us of a network of weak interactions that solute and solvent molecules could be engaged in. The π/π-stacking and the intramolecular H-bonding interactions among stacks of dithranol molecules in the crystalline state were utilized to create structures for various solute/solvent pairing.

The level of theory in our study was chosen by considering the results of high-level, *ab initio* wave function calculations carried out by others for and extensive set of anthrone and related hydroxyarene molecules using the CBS-QB3 level of theory.[28,29] Table S2 summarizes the calculated deviations in relative isomer energies between the reference *ab initio* wave function level and representative pure GGA (BP86,[30,31] BLYP,[31,32] and PBE:[33,34] Rung 2), metaGGA (TPSS,[35] revised TPSS,[36,37] and M06L:[38] Rung 3), and hyperGGA (B3LYP,[32,39] cam-B3LYP+GB3J,[40,41] ωB97xD,[42,43] and MN15:[16] Rung 4) density functionals. While qualitatively all functionals predicted the correct energetic order of dithranol isomers, we found a significant improvements in the absolute relative energy values (within +4.0 kJ/mol error) when using MN15[16] functional with triple-ζ basis set supplemented with both polarization and diffuse functions for all heavy and light atoms (6-311++G**).[17–19] Moreover, we also evaluated the performance of three implicit solvation models (PCM,[44] COSMO,[45] and SMD[20]) using solvent parameters reported in Table S1. We found that only the SMD polarizable continuum model with electrostatic solvent/solute and non-electrostatic solvent/solvent interactions for the $CHCl_3$ and DMSO solutions provide negative solvation energy of the solvent molecule itself. Thus, our validated level of theory employed implicitly and explicitly solvated model calculations is the MN15[16]/6-311++G**[17–19]/PCM(SMD[20]). This particular combination of level of theory and solvation model is notable given that they were developed by the same team of scientists that ensures a degree of self-consistency.

All reported optimized geometries were confirmed to correspond to equilibrium structures by vibrational analysis showing no imaginary normal modes with the exception of transient state structure with constrained intermolecular distances. These frequency calculations also provided us with the predicted IR vibrational spectra that clearly showed the significant overlap of the C=O and aromatic C=C stretching modes. This prevents employing FTIR as a diagnostic technique for differentiating among various tautomers. Given that our thesis is the critical influence of solvents on relative energies of substrate isomers, we supplemented the standard thermochemical calculations with translational entropy correction for a solute at 100 μM concentration in various solvents, as proposed by Whitesides.[24] In brief, we determined the 'effective solute concentration' in the space of the solution that is available for the solute and not excluded by the solvent molecules. The overestimation of translational entropy using the ideal gas phase model can be as much as 30%. The translational entropy of a solute was then calculated using the equation $S^{\mathrm{trans,corr}} = 11.1 + 12.5\ \ln(M_{\mathrm{w}}^{\mathrm{solute}}) + 12.5$

$\ln(T) - 8.1 \ln([\text{analyte}]^{\text{eff.}})$. The numerical details of the translational entropy corrections are summarized in Table S4.

ASSOCIATED CONTENT

Supporting Information. Computational models, validations of the level of theory, UV/vis and fluorescence spectral data and fits, and UV/vis and HPLC data monitoring dithranol reactions are included in the supporting information. This material is available free of charge via the Internet at http://pubs.acs.org. Additional electronic supporting information is available at the free, publically accessible Zenodo dataset depository, DOI: 10.5281/zenodo.3554508. This includes downloadable files containing the atomic positions of each tautomer considered, validation of several density functionals, and detailed worksheet for correcting calculated free energy with condensed phase translation entropy.

AUTHOR INFORMATION

*Corresponding author information: jennifer.dubois1@montana.edu (JLD); szilagyi@montana.edu (RKSz). ORCID JLD: 0000-0001-5593-3391 and RKSz: 0000-0002-9314-6222

Acknowledgement. We thank Dr. Brian Tripet of the Montana State University NMR facility for his assistance in measuring, plotting, and interpreting NMR spectral data. The NMR facility was funded by the NSF-Major Research Instrumentation program (NSF-MRI: DBI-1532078), the Murdock Charitable Trust Foundation (015066:MNL), and support from the MSU Vice-President for Research and Economic Development office. We thank Garrett Moraski for helpful discussions. Financial support for this work is from the US National Science Foundation grant MCB1715176. No competing financial interests have been declared.

REFERENCES & ENDNOTES

(1) Que, L. Q. J.; Valentine, J. S. Oxygen Metabolism. In Bioinorganic Chemistry; Bertini, I., Gray, H. B., Stiefel, E. I., Valentine, J. S., Eds.; University Science Books: Sausalito, CA, 2007; Vol. 207.

(2) Mano, N.; de Poulpiquet, A. O2 Reduction in Enzymatic Biofuel Cells. Chem. Rev. 2018, 118, 2392–2468. https://doi.org/10.1021/acs.chemrev.7b00220.

(3) McDonald, C. A.; Fagan, R. L.; Collard, F.; Monnier, V. M.; Palfey, B. A. Oxygen Reactivity in Flavoenzymes: Context Matters. J. Am. Chem. Soc. 2011, 133, 16809–16811. https://doi.org/10.1021/ja2081873.

(4) Fetzner, S.; Steiner, R. A. Cofactor-Independent Oxidases and Oxygenases. Appl. Microbiol. Biotechnol. 2010, 86, 791–804. https://doi.org/10.1007/s00253-010-2455-0.

(5) Hernandez-Ortega, A.; Quesne, M. G.; Bui, S.; Heuts, D. P. H. M.; Steiner, R. A.; Heyes, D. J.; De Visser, S. P.; Scrutton, N. S. Origin of the Proton-Transfer Step in the Cofactor-Free (1H)-3-Hydroxy-4-Oxoquinaldine 2,4-Dioxygenase: Effect of the Basicity of an Active Site His Residue. J. Biol. Chem. 2014, 289, 8620–8632. https://doi.org/10.1074/jbc.M113.543033.

(6) Machovina, M. M.; Usselman, R. J.; Du Bois, J. L. Monooxygenase Substrates Mimic Flavin to Catalyze Cofactorless Oxygenations. J. Biol. Chem. 2016, 291, 17816–17828. https://doi.org/10.1074/jbc.M116.730051.

(7) Machovina, M. M.; Ellis, E. S.; Carney, T. J.; Brushett, F. R.; DuBois, J. L. How a Cofactor-Free Protein Environment Lowers the Barrier to O2 Reactivity. J. Biol. Chem. 2019, 294, 3661-3669. https://doi.org/10.1074/jbc.RA118.006144.

(8) Ylihonko, K.; Tuikkanen, J.; Jussila, S.; Cong, L.; Mäntsälä, P. A Gene Cluster Involved in Nogalamycin Biosynthesis from Streptomyces Nogalater: Sequence Analysis and Complementation of Early-Block Mutations in the Anthracycline Pathway. Mol. Gen. Genet. 1996, 251, 113–120. https://doi.org/10.1007/s004380050147.

(9) Koskiniemi, H.; Grocholski, T.; Schneider, G.; Niemi, J. Expression, Purification and Crystallization of the Cofactor-Independent Monooxygenase SnoaB from the Nogalamycin Biosynthetic Pathway. Acta Crystallogr. Sect. F Struct. Biol. Cryst. Commun. 2009, 65, 256–259. https://doi.org/10.1107/S1744309109001389.

(10) Grocholski, T.; Koskiniemi, H.; Lindqvist, Y.; Mäntsälä, P.; Niemi, J.; Schneider, G. Crystal Structure of the Cofactor-Independent Monooxygenase SnoaB from *Streptomyces nogalater* : Implications for the Reaction Mechanism. Biochemistry 2010, 49, 934–944. https://doi.org/10.1021/bi901985b.

(11) Müller, K. Antipsoriatic Anthrones: Aspects of Oxygen Radical Formation, Challenges and Prospects. Gen. Pharmacol. 1996, 27, 1325–1335. https://doi.org/10.1016/S0306-3623(96)00075-4.

(12) Hernández-Ortega, A.; Quesne, M. G.; Bui, S.; Heyes, D. J.; Steiner, R. A.; Scrutton, N. S.; De Visser, S. P. Catalytic Mechanism of Cofactor-Free Dioxygenases and How They Circumvent Spin-Forbidden Oxygenation of Their Substrates. J. Am. Chem. Soc. 2015, 137, 7474–7487. https://doi.org/10.1021/jacs.5b03836.

(13) Cantú Reinhard, F. G.; DuBois, J. L.; De Visser, S. P. Catalytic Mechanism of Nogalamycin Monoxygenase: How Does Nature Synthesize Antibiotics without a Metal Cofactor? J. Phys. Chem. B 2018, 122, 10841–10854. https://doi.org/10.1021/acs.jpcb.8b09648.

(14) Korth, H.-G.; Mulder, P. Anthrone and Related Hydroxyarenes: Tautomerization and Hydrogen Bonding. J. Org. Chem. 2013, 78, 7674–7682. https://doi.org/10.1021/jo401243b.

(15) Note: Two lines of evidence suggest that the enzyme pocket contributes to substrate activation and reaction beyond facilitating the initial deprotonation. First, at pH values below the pK_a, the enzymatic process still occurs at a rate that exceeds the rate of uncatalyzed oxidation (see ref. 6). Second, the spontaneous reaction with O_2 even in neat DMF is still several orders of magnitude slower than in the NMO-dithranolate$^-$ complex, indicating that the enzyme serves an additional catalytic role in converting the ion-pair [dithranolate$^-$ + O_2] to the radical-pair [dithranyl•/O_2•$^-$], likely involving lowering the reorganization energy associated with electron transfer (see ref. 7).

(16) Yu, H. S.; He, X.; Li, S. L.; Truhlar, D. G. MN15: A Kohn-Sham Global-Hybrid Exchange-Correlation Density Functional with Broad Accuracy for Multi-Reference and Single-Reference Systems and Noncovalent Interactions. Chem. Sci. 2016, 7, 5032–5051. https://doi.org/10.1039/c6sc00705h.

(17) Krishnan, R.; Binkley, J. S.; Seeger, R.; Pople, J. A. Self-Consistent Molecular-Orbital Methods 20. Basis Set for Correlated Wave-Functions. J. Chem. Phys. 1980, 72, 650–654.

(18) McLean, A. D.; Chandler, G. S. Contracted Gaussian Basis Sets for Molecular Calculations. I. Second Row Atoms, Z=11-18. J. Chem. Phys. 1980, 72, 5639–5648. https://doi.org/10.1063/1.438980.

(19) Frisch, M. J.; Pople, J. A.; Binkley, J. S. Self-Consistent Molecular-Orbital Methods 25.

Supplementary Functions for Gaussian-Basis Sets. J. Chem. Phys. 1984, 80, 3265–3269.

(20) Marenich, A. V.; Cramer, C. J.; Truhlar, D. G. Universal Solvation Model Based on Solute Electron Density and on a Continuum Model of the Solvent Defined by the Bulk Dielectric Constant and Atomic Surface Tensions. J. Phys. Chem. B 2009, 113, 6378–6396. https://doi.org/10.1021/jp810292n.

(21) Marenich, A. V.; Kelly, C. P.; Thompson, J. D.; Hawkins, G. D.; Chambers, C. C.; Giesen, D. J.; Winget, P.; Cramer, C. J.; Truhlar, D. G. Minnesota Solvation Database. University of Minnesota: Minneapolis 2012.

(22) Gadda, G. Oxygen Activation in Flavoprotein Oxidases: The Importance of Being Positive. Biochemistry 2012, 51, 2662–2669. https://doi.org/10.1021/bi300227d.

(23) Ahmed, F. R. The Correct Structural Formula for Anthralin. Acta Crystallogr. Sect. B Struct. Crystallogr. Cryst. Chem. 1980, 36, 3184–3186. https://doi.org/10.1107/s0567740880011247.

(24) Whitesides, G. M.; Mammen, M.; Shakhnovich, E. I.; Deutch, J. M. Estimating the Entropic Cost of Self-Assembly of Multiparticle Hydrogen-Bonded Aggregates Based on the Cyanuric Acid Center Dot Melamine Lattice. J. Org. Chem. 1998, 63, 3821–3830.

(25) Campbell, A. N.; Stahl, S. S. Overcoming the “Oxidant Problem”: Strategies to Use O2 as the Oxidant in Organometallic C-H Oxidation Reactions Catalyzed by Pd (and Cu). Acc. Chem. Res. 2012, 45, 851–863. https://doi.org/10.1021/ar2002045.

(26) Note: Care must be taken to avoid contact between these solutions (or any solution of dithranol in an organic solvent) with rubbers, plastics, epoxies, etc., which were observed to degrade rapidly.

(27) Groom, C. R.; Bruno, I. J.; Lightfoot, M. P.; Ward, S. C. The Cambridge Structural Database. Acta Crystallogr. Sect. B Struct. Sci. Cryst. Eng. Mater. 2016, 72, 171–179. https://doi.org/10.1107/S2052520616003954.

(28) Montgomery, J. A.; Frisch, M. J.; Ochterski, J. W.; Petersson, G. A. A Complete Basis Set Model Chemistry. VI. Use of Density Functional Geometries and Frequencies. J. Chem. Phys. 1999, 110, 2822–2827. https://doi.org/10.1063/1.477924.

(29) Montgomery, J. A.; Frisch, M. J.; Ochterski, J. W.; Petersson, G. A. A Complete Basis Set Model Chemistry. VII. Use of the Minimum Population Localization Method. J. Chem. Phys. 2000, 112, 6532–6542. https://doi.org/10.1063/1.481224.

(30) Perdew, J. P. Density-Functional Approximation for the Correlation Energy of the Inhomogeneous Electron Gas. Phys. Rev. B 1986, 33, 8822–8824. https://doi.org/10.1103/PhysRevB.33.8822.

(31) Becke, A. D. Density-Functional Exchange-Energy Approximation with Correct Asymptotic Behavior. Phys. Rev. A 1988, 38, 3098–3100. https://doi.org/10.1103/PhysRevA.38.3098.

(32) Lee, C.; Yang, W.; Parr, R. G. Development of the Colle-Salvetti Correlation-Energy Formula into a Functional of the Electron Density. Phys. Rev. B 1988, 37, 785–789. https://doi.org/10.1103/PhysRevB.37.785.

(33) Perdew, J. P.; Burke, K.; Ernzerhof, M. Generalized Gradient Approximation Made Simple. Phys. Rev. Lett. 1996, 77, 3865–3868. https://doi.org/10.1103/PhysRevLett.77.3865.

(34) Perdew, J. P.; Ernzerhof, M.; Burke, K. [ERRATUM] Generalized Gradient Approximation Made Simple. Phys. Rev. Lett. 1997, 78, 1396-1396. https:// DOI: 10.1103/PhysRevLett.78.1396.

(35) Staroverov, V. N.; Scuseria, G. E.; Tao, J.; Perdew, J. P. Comparative Assessment of a New Nonempirical Density Functional: Molecules and Hydrogen-Bonded Complexes. J. Chem. Phys. 2003, 119, 12129–12137. https://doi.org/10.1063/1.1626543.

(36) Perdew, J. P.; Ruzsinszky, A.; Csonka, G. I.; Constantin, L. A.; Sun, J. Workhorse Semilocal Density Functional for Condensed Matter Physics and Quantum Chemistry. Phys. Rev. Lett. 2009, 103, 1-4. https://doi.org/10.1103/PhysRevLett.103.026403

(37) Perdew, J. P.; Ruzsinszky, A.; Csonka, G. I.; Constantin, L. A.; Sun, J. [ERRATUM] Workhorse Semilocal Density Functional for Condensed Matter Physics and Quantum Chemistry. Phys. Rev. Lett. 2011, 106, 1-1. https://doi.org/10.1103/PhysRevLett.106.179902,

(38) Y. Zhao; D. G. Truhlar. A New Local Density Functional for Main-Group Thermochemistry, Transition Metal Bonding, Thermochemical Kinetics, and Noncovalent Interactions. J. Chem. Phys. 2006, 125, 1–18. https://doi.org/10.1063/1.2370993.

(39) Becke, A. D. Density-Functional Thermochemistry. III. The Role of Exact Exchange. J. Chem. Phys. 1993, 98, 5648–5652. https://doi.org/10.1063/1.464913.

(40) Yanai, T.; Tew, D. P.; Handy, N. C. A New Hybrid Exchange-Correlation Functional Using the Coulomb-Attenuating Method (CAM-B3LYP). Chem. Phys. Lett. 2004, 393, 51–57. https://doi.org/10.1016/j.cplett.2004.06.011.

(41) Grimme, S.; Ehrlich, S.; Goerigk, L. Effect of the Damping Function in Dispersion Corrected Density Functional Theory. J. Comput. Chem. 2011, 32, 1456–1465. https://doi.org/10.1002/jcc.21759.

(42) Chai, J. Da; Head-Gordon, M. Systematic Optimization of Long-Range Corrected Hybrid Density Functionals. J. Chem. Phys. 2008, 128, 084106. https://doi.org/10.1063/1.2834918.

(43) Chai, J. Da; Head-Gordon, M. Long-Range Corrected Hybrid Density Functionals with Damped Atom-Atom Dispersion Corrections. Phys. Chem. Chem. Phys. 2008, 10, 6615–6620. https://doi.org/10.1039/b810189b.

(44) Scalmani, G.; Frisch, M. J. Continuous Surface Charge Polarizable Continuum Models of Solvation. I. General Formalism. J. Chem. Phys. 2010, 132, 1-15. https://doi.org/10.1063/1.3359469.

(45) Barone, V.; Cossi, M. Quantum Calculation of Molecular Energies and Energy Gradients in Solution by a Conductor Solvent Model. J. Phys. Chem. A 1998, 102, 1995–2001. https://doi.org/10.1021/jp9716997.

TABLE OF CONTENTS/GRAPHICAL ABSTRACT FIGURE: